

Searching for the Essence of Adversarial Perturbations

Dennis Y. Menn and Hung-yi Lee

College of Electrical Engineering and Computer Science, National Taiwan University

DennisYMenn@gmail.com, hungyilee@ntu.edu.tw

Abstract

Neural networks have achieved the state-of-the-art performance in various machine learning fields, yet the incorporation of malicious perturbations with input data (adversarial example) is shown to fool neural networks' predictions. This would lead to potential risks for real-world applications such as endangering autonomous driving and messing up text identification. To mitigate such risks, an understanding of how adversarial examples operate is critical, which however remains unresolved. Here we demonstrate that adversarial perturbations contain human-recognizable information, which is the key conspirator responsible for a neural network's erroneous prediction, in contrast to a widely discussed argument that human-imperceptible information plays the critical role in fooling a network. This concept of human-recognizable information allows us to explain key features related to adversarial perturbations, including the existence of adversarial examples, the transferability among different neural networks, and the increased neural network interpretability for adversarial training. Two unique properties in adversarial perturbations that fool neural networks are uncovered: masking and generation. A special class, the complementary class, is identified when neural networks classify input images. The human-recognizable information contained in adversarial perturbations allows researchers to gain insight on the working principles of neural networks and may lead to develop techniques that detect/defense adversarial attacks.

Introduction

The application of image recognition has been tightly woven into our daily life. Commonly encountered examples include the text identification of license plates, facial recognition, medical image analysis, defect detection in manufacturing industry, and autonomous vehicles. It can be expected that many more applications will be realized in the near future. However, just like a computer virus damaging/destroying a software/hardware system, adversarial attack tricks a neural network to erroneously categorize an image. A likely consequence is that someone will be waiting to crash a self-driving car through adversarial attack (Eykholt et al. 2018). Thus preventing adversarial attack from happening is critical to the successful application of image recognition. Again, similar to the computer virus that knowing how the virus works is the first step to prevent its malicious attack,

understanding the working principles of the adversarial attack is critical to counter its intended mischief. Despite this topic having been intensely studied since the discovery of adversarial perturbations in 2013 (Szegedy et al. 2014), the reason for having adversarial examples, to our best knowledge, is yet to be resolved.

For a neural network to correctly classify an image, it must emphasize recognizable characteristics of the image by placing large gradient values on, for examples, tires of a car, wings of a plane, and the shape of an object (Simonyan, Vedaldi, and Zisserman 2014; Smilkov et al. 2017). Hence, a slightly change of pixel values in these characteristics can greatly modify the neural network's outcome. Consequently, we would assume that, for adversarial perturbations to confuse neural networks, changing pixel values of recognizable characteristics in an image is critical. This leads us to postulate that *adversarial perturbations contain human-recognizable information*. After all, the usefulness of neural network is judged by human. This human-recognizable information is the key conspirator responsible for neural networks' erroneous predictions.

The perceptible information contained in adversarial perturbations is generally incomplete and, worse yet, corrupted by heavy noise. This makes the identification of perceptible information challenging and non-intuitive. Adversarial perturbations are noisy because neural network's gradients of the class score are noisy, and perturbations are often derived from the gradients. Since the neural network does not need to utilize all the information in an image to correctly classify the image, adversarial perturbations need not to have, for example, the complete shape of a car, to fool the network successfully. This implies that adversarial perturbations with incomplete characteristics occur naturally, contributing to the difficulty for human to recognize adversarial perturbations. In addition, our unfamiliarity with the working principle of neural networks, a wide variety of attack algorithms, and different attack scenarios all contribute to the complexity of the topic.

To verify our postulate that adversarial perturbations contain human-recognizable information, we need to minimize the effect of noise and find a way to recreate recognizable characteristics. Importantly, when processing adversarial

perturbations, the ability to attack neural networks must not be lost. We have obtained perturbations from different neural networks and averaged them. The reason for averaging is because both the noise and the incomplete characteristics are likely to be independent for different neural networks. Averaging would not only minimize the effect of the noise but also put together different parts of recognizable characteristics. However, the number of available neural networks is often limited and averaging limited number of adversarial perturbations from different neural networks cannot achieve the desired goals. Inspired by SmoothGrad (Smilkov et al. 2017), we incorporate Gaussian noise $N(0, \sigma^2)$, with mean 0 and standard deviation σ , with n copies of the input image x and calculated the adversarial perturbations, V_i , for the neural network i to increase the number of perturbations. Then we average the adversarial perturbations over n copies and m different neural networks. Mathematically, this is

$$V(x) = \frac{1}{mn} \sum_{i=1}^m \sum_{j=1}^n V_i(x + N_j(0, \sigma^2)). \quad (1)$$

We have examined our postulate for different attack algorithms on MNIST (LeCun and Cortes 2010) and CIFAR10 (Krizhevsky and Hinton 2009) datasets. We have qualitatively measured how recognizable the characteristics in adversarial perturbations really are and made several interesting discoveries. In addition, we have found that our postulate is able to successfully explain key features in adversarial perturbations (to be discussed below) and the application of this concept would allow us to devise methods to counter adversarial attacks against image recognition.

Related Work

Neural networks have achieved the state-of-the-art performance in various machine learning tasks (Krizhevsky, Sutskever, and Hinton 2012; Hinton et al. 2012; LeCun, Bengio, and Hinton 2015). However, Szegedy et al. have found that small perturbations incorporated with input images are sufficient to fool neural network’s judgement (Szegedy et al. 2014). These small perturbations, adversarial perturbations, increase the prediction error made by neural networks, which is often done by refining adversarial perturbations iteratively through backpropagation (Rumelhart, Hinton, and Williams 1986) to optimize a preset loss function. In practice, a number of attack algorithms have shown to attain this goal (Goodfellow, Shlens, and Szegedy 2015; Kurakin, Goodfellow, and Bengio 2017; Madry et al. 2018; Moosavi-Dezfooli, Fawzi, and Frossard 2016; Carlini and Wagner 2017; Papernot et al. 2016; Moosavi-Dezfooli et al. 2017).

Four well-known features of adversarial perturbations are (Akhtar et al. 2021): (1) Neural network’s vulnerability against adversarial perturbations: Though often impercepti-

ble to human, adversarial perturbations are sufficient to affect neural network’s performance when incorporated with images (Szegedy et al. 2014). (2) Transferability: Perturbations crafted for one neural network can often, surprisingly, fool neural networks with different architectures (Szegedy et al. 2014). Furthermore, adversarial examples can even be misclassified by neural networks trained on different datasets (Szegedy et al. 2014; Papernot, McDaniel, and Goodfellow 2016). (3) Adversarial training improving neural network’s interpretability: Neural network’s gradient of the score of the labelled class and produced adversarial perturbations are often incomprehensible (Simonyan, Vedaldi, and Zisserman 2014; Goodfellow, Shlens, and Szegedy 2015), they become recognizable to human after adversarial training (Goodfellow, Shlens, and Szegedy 2015; Ross and Doshi-Velez 2018; Tsipras et al. 2019; Santurkar et al. 2019). (4) Non-trivial accuracy for classifiers trained by a perturbed dataset: A neural network trained on a dataset, which is composed of images incorporated with targeted adversarial perturbations and relabeled as the target class, has demonstrated an accuracy up to 63.3% on CIFAR10’s testing set (Ilyas et al. 2019).

Understanding above features not only benefits in devising effective defensive algorithms but also sheds light on the working principles of neural networks, which is often regarded as a black box. Several works have attempted to unveil the nature of adversarial perturbations, yet a consensus is still lacking. Those works include the overly linearity of neural networks (Goodfellow, Shlens, and Szegedy 2015; Tramèr et al. 2017), adversarial examples off the data manifold (Tanay and Griffin 2016; Song et al. 2018; Samangouei et al. 2018), adversarial perturbations modifying non-robust features (Schmidt et al. 2018; Tsipras et al. 2019; Ilyas et al. 2019), and identifying fundamental bounds on the susceptibility of a classifier (Schmidt et al. 2018; Shafahi et al. 2019). In contrast to those works, in the following we establish the fact that adversarial perturbations contain human-recognizable information which is the key conspirator for fooling neural networks.

Properties of Adversarial Perturbations

Two distinctive properties of adversarial perturbations have been observed in this work. The first resembles the negative of recognizable characteristics in an input image. Incorporating this property with an image results in the subtraction of the pixel values of recognizable characteristics from the input image, thus lowering the value of the inner product between the gradient of the labelled-class score and the input image. We refer this property as *masking*.

The second property relates to the emergence of new characteristics in adversarial perturbations. The incorporation of the new characteristics to an image can make both human and a neural network to wrongly classify the image. We refer this property as *generation*.

Masking is easier to observe compared to generation because masking refers to existing characteristics in an image whereas features by generation do not necessarily follow the image’s profile. As an example, a car’s shape and tires are critical for identifying its class, so adversarial perturbations from different neural networks will show similar masking features. However, there is more than one way to turn a car into a plane by adding different features to the car. Thus, adversarial perturbations from different neural networks would show different generation features. We will illustrate the effects of masking and generation below.

Experimental Setup

In the experiment, neural networks are divided into two categories: source models and testing models. Source models are used to produce adversarial perturbations and testing models for evaluation. We obtain adversarial perturbations through two different settings: (1) The single-model setting (SM): Adversarial perturbations are produced in the usual way, i.e., sending one image to a source model and obtain the corresponding adversarial perturbations. (2) The multiple-models setting with Gaussian noise (MM+G): Adversarial perturbations are obtained according to Eqn. (1). We have examined BIM attack (Kurakin, Goodfellow, and Bengio 2017), CW attack (Carlini and Wagner 2017), and DeepFool attack (Moosavi-Dezfooli, Fawzi and Frossard 2016) for both untargeted and targeted attack mode on CIFAR10 and MNIST datasets (Note that DeepFool does not have targeted attack mode.). To visualize adversarial perturbations under untargeted attack mode, we first multiple them by -1 since masking denotes the negative of recognizable characteristics. We then scale the mean and variance of perturbations to dataset’s mean and variance. Detailed information about experimental setup is listed in Supplementary Material.

Untargeted Attack

Figure 1(a) shows input images from CIFAR10 and MNIST. Figure 1 (b), (d), and (f) [(c), (e), and (g)] display the negatives of the perturbations from SM [MM+G] for three attack algorithms BIM, CW, and DeepFool, respectively. The process of generating perturbations with MM+G, compared with those with SM, minimizes the background noise and recreates the recognizable characteristics efficiently. Indeed, human-recognizable information emerges in the perturbations, demonstrating the effect of masking. Furthermore, perturbations with definitive characteristics and a very low noise background produced by CW attack with MM+G, shown in Figure 1(e), display a high strength to attack neural networks (to be discussed in Table 2). This demonstrates that masking, not noise, is central for fooling neural networks.

For the car and bird images, columns 1 and 2 in Figure 1, respectively, recognizable characteristics in the perturbations resemble the shape of the input images, whereas those for the dog image, column 3 in Figure 1, resemble its face only. This implies that perturbations possessing only a portion of an object’s characteristics are sufficient for a successful attack.

For MNIST dataset under SM, contours of digits are already observable in adversarial perturbations, as shown in Figure 1. MM+G displays better-shaped digits with low background noise, with the exception of CW attack where SM already has a low background noise. Interestingly, the adversarial perturbations also show the effect of generation for MNIST dataset. The perturbations for digit 1 display a fuzzy 4 and a clear 7 for BIM and CW attack under MM+G, respectively. More prominent consequences of generation can be seen later in the targeted attack mode.

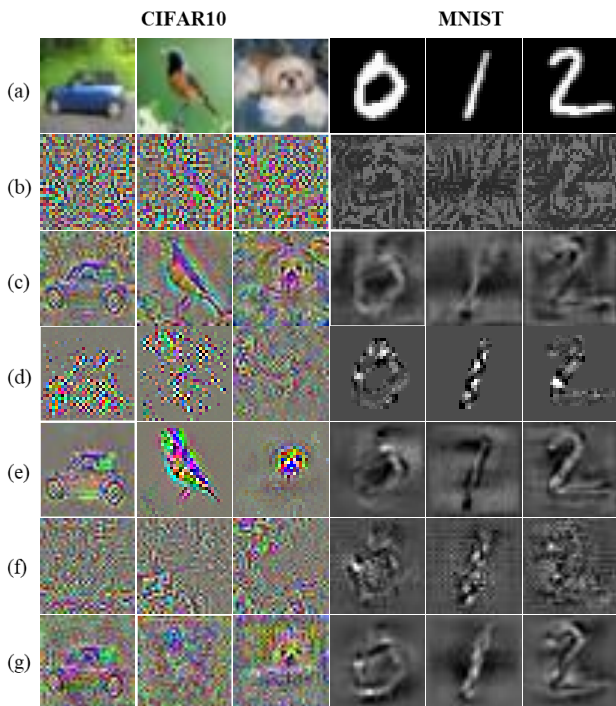


Figure 1: Adversarial perturbations produced under SM and MM+G in the untargeted attack mode for images from CIFAR10 and MNIST datasets. (a) Input images. (b), (d), and (f) [(c), (e), and (g)]: Perturbations under SM [MM+G] from BIM, CW, and DeepFool attacks, respectively. Clear recognizable characteristics emerge under MM+G for both datasets. Adversarial perturbations from CW attack under MM+G for CIFAR10 show clear contours with low background noise. These perturbations of small magnitudes are capable of confusing a neural network’s classification, illustrating the effect of masking. Only three for a total of ten classes in each dataset are shown. Six of the seven unshown classes have similar behaviors with the exception of the class of cat.

Evaluating Perceptibility

In order to quantitatively measure how recognizable the effect of masking in adversarial perturbations really is, we first obtain adversarial perturbations under SM and MM+G. For MNIST, we multiply the perturbations by -1 to cancel the negative sign of masking and change the modified values that exceed 5×10^{-6} to 1 and other values to 0 because pixel values are mostly 0 and 1 in MNIST. For CIFAR10, we scale the values of adversarial perturbations, the same as how we scale adversarial perturbations for the purpose of visualization. Then we multiply the adversarial perturbations by 0.05 after scaling to enhance testing model’s classification accuracy. Because we expect the effect of masking resemble the input images, the label of each perturbations is set to be identical to that of the input image. Then we send the perturbations to testing models to evaluate the classification accuracy.

Testing models predict up to 60% accuracy of the respective labelled classes of input images for CIFAR10 and MNIST (10 classes in each dataset). This confirms that masking resembles the recognizable characteristics in the input image, demonstrating the strong perceptibility of these perturbations, as shown in Table 1. Note that only ~10% accuracy, i.e., random guessing, under SM for CIFAR10, a clear sign that unprocessed perturbations are not recognizable. It is noted that DeepFool shows inferior accuracy in CIFAR10. This inferiority may stem from its algorithm being halted as soon as the source model misclassifies the input image, so the produced adversarial perturbations are often far from being optimal.

Setting	SM			MM+G		
Attack alg.	BIM	CW	DeepFool	BIM	CW	DeepFool
DenseNet	0.10	0.10	0.10	0.59	0.47	0.11
Dia-ResNet	0.07	0.14	0.08	0.73	0.39	0.33
PyramidNet	0.09	0.07	0.11	0.68	0.55	0.19
ResNet	0.09	0.09	0.10	0.52	0.43	0.21
Avg.	0.09	0.10	0.10	0.63	0.46	0.21

Table 1a Perceptibility for CIFAR10

Setting	SM			MM+G		
Attack alg.	BIM	CW	DeepFool	BIM	CW	DeepFool
Testing model	0.18	0.46	0.17	0.57	0.44	0.68

Table 1b Perceptibility for MNIST

Table 1: Perceptibility measurements of CIFAR10 and MNIST datasets. The element e_{ij} in the table represents the i^{th} testing model’s classification accuracy of the perturbations from the j^{th} attack algorithm. Under SM for CIFAR10,

testing model’s classification accuracy is similar to that of random guessing, 0.1. Since the contour of digits are already observable under SM for MNIST, the classification accuracy can get up to 46%. Under MM+G, the testing model’s accuracy for both CIFAR10 and MNIST can exceed 60%, which indicates that the recognizable characteristics in perturbations are strongly recognizable.

Evaluating Attack Strength

To verify if adversarial perturbations obtained from MM+G is still capable of attacking neural networks, we evaluate the attack strength. We have produced adversarial perturbations for selected data under SM and MM+G. Then, we have processed the perturbations by multiplying a quantity ε with their signs, as shown below:

$$V' = \varepsilon \cdot \text{sign}(V). \quad (2)$$

Here V and V' are the original and processed adversarial perturbations respectively, $\varepsilon = 0.2$ for MNIST and $\varepsilon = 0.03$ for CIFAR10. This procedure is similar to that of fast gradient sign method (Goodfellow, Shlens, and Szegedy 2015); every perturbation has the same L_{inf} norm and L_2 norm. Next, we have incorporated the processed perturbations with the input images and sent to testing models to evaluate the accuracy of classification. Please refer to Supplementary Material for further discussion on processing perturbations.

Testing models get fooled by the incorporation of processed adversarial perturbations with input images, as demonstrated in Table 2. The attack strengths of the adversarial examples obtained from three attack algorithms for CIFAR10 and MNIST are listed in Table 2a and 2b, respectively. In the image column of Table 2a, testing models correctly classify 94%, on average, of input images. The effect of adding noise, defined as a random sampling where each pixel value has an equal probability of being $+\varepsilon$ or $-\varepsilon$, to images results in a decrease of the classification accuracy to 82% (noise column). Incorporation of perturbations under SM makes the classification accuracy drop, on average, to 39% for BIM attack. Perturbations from MM+G further reduces the classification accuracy. For CW attack the classification accuracy drops down to 12% on average, slightly larger than the random guessing of 10%. This confirms the strong ability of masking in attacking neural networks. In Table 2b the accuracy is or approaches 0 for all attack algorithms under MM+G. An expected trend of increased attack strength from SM to MM+G is observed for both datasets.

We have found that adversarial examples obtained from three attack algorithms under MM+G and processed by Eqn. (2) show detectable differences from input image. The differences are not significant enough to influence human’s judgement on classifying individual images, yet sufficient to fool testing models (Supplementary Material).

Setting	Reference		SM			MM+G		
Attack alg. Testing model	Image	Noise	BIM	CW	DeepFool	BIM	CW	DeepFool
DenseNet	0.92	0.77	0.33	0.52	0.44	0.13	0.09	0.34
Dia-ResNet	0.96	0.9	0.51	0.72	0.68	0.31	0.22	0.56
PyramidNet	0.94	0.79	0.33	0.53	0.57	0.18	0.09	0.39
ResNet	0.92	0.8	0	0.14	0.21	0.21	0.09	0.4
Avg.	0.94	0.82	0.39	0.59	0.56	0.21	0.12	0.42

Table 2a: Attack strength for CIFAR10

Setting	Reference		SM			MM+G		
Attack alg. Testing model	Image	Noise	BIM	CW	DeepFool	BIM	CW	DeepFool
Testing model	1	0.88	0.03	0.56	0.15	0	0.03	0

Table 2b Attack strength for MNIST

Table 2: Attack strength of adversarial perturbations processed by MM+G. Values under “Image” column represent classification accuracies on clean images and those of “Noise” are accuracies after incorporating noise with images. The element e_{ij} represents the classification accuracy for the testing model i under the attack algorithm j . In Table 2a, ResNet is the same for both source model and testing model under SM in CIFAR10, the so-called white-box attack. Values obtained from ResNet are excluded from calculating values in the row of “Avg.” under SM. Four testing models are employed in Table 2a. Testing model employed in Table 2b is described in Supplementary Material.

Observations

The utilization of MM+G allows us to not only see literally the recognizable aspect of adversarial perturbations but also preserve the strong attack ability on neural networks. Four noteworthy observations under untargeted attack are summarized below:

(1) Discrepancies between input images and perturbations We have placed the input image and the corresponding adversarial perturbation side by side to find differences between the two. Interestingly, the shapes of recognizable characteristics in adversarial perturbations often show discrepancies compared to those of input images. For example, in Figure 1 the bird’s tail produced from BIM attack is longer than that of the input image. The boundaries of recognizable characteristics can also be different. Halos enclosing the boundaries of the objects of interest have been observed in many perturbations, as shown for the car and the bird in Figure 1. The exact cause for the halos remains to be identified.

(2) Aligning of perturbations among different attack algorithms

Although discrepancies between input images and adversarial perturbations exist, the shapes and boundaries of adversarial perturbations from different attack algorithms align well. For example, produced separately from BIM and CW attacks, the boundaries of the two cars are almost identical and those of the two birds, except the lengths of the tails, also have a good alignment, as shown in Figure 1.

(3) Background streaks/wringers in adversarial perturbations

Background streaks/wringers emerge in some of the perturbations produced by BIM and DeepFool attack, as shown in Figure 2. It is puzzling that different models would show similar streaks/wringers unrelated to the input image.

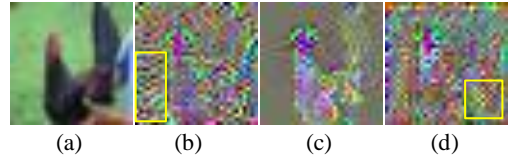


Figure 2: Streaks/wringers appearing in adversarial perturbations. (a) Input image. (b), (c), and (d): Adversarial perturbations from BIM, CW, and DeepFool attacks, respectively. Streaks/wringers are marked by yellow rectangles. This phenomenon is not obvious in CW attack.

(4) The missing cat

The images of adversarial perturbations for the class of cats in CIFAR10 are difficult to recognize, as shown in Figure 3, yet the corresponding adversarial perturbations are still classified as cat by testing models. To investigate further, we have sent 100 Gaussian noises, with mean and variance being the same as that of the CIFAR10 dataset, to testing models for classification. Interestingly, the classification of the Gaussian noises is highly concentrated on either bird or cat for four different testing models, as shown in Table 3. A similar situation has also been found in MNIST with the class being digit 8.

We contemplate that, for an input image does not mimic the characteristics subscribed by individual classes, the neural network will classify it as a specific class with a high probability, like the classes of cat and bird in the above example. Because images of cats and birds in the training dataset have a wide range of shapes and postures, networks are inherently difficult to pick up identifiable characteristics. Consequently, neural networks develop a strategy to only classify the other eight classes and pick up the class of cat or bird for images not recognizable by the networks. We designate this class as the “complementary class”.



Figure 3: The missing cat. (a) Input images of cats from CIFAR10. (b) Adversarial perturbations from BIM attack under MM+G. Despite unrecognizable adversarial perturbations, testing models still classify these perturbations as cat.

Testing model \ Class	Class									
	Plane	Car	Bird	Cat	Deer	Dog	Frog	Horse	Ship	Truck
DenseNet	0	0	0	1	0	0	0	0	0	0
Dia-ResNet	0	0	0.23	0.77	0	0	0	0	0	0
PyramidNet	0	0	0.05	0.95	0	0	0	0	0	0
ResNet	0	0	1	0	0	0	0	0	0	0

Table 3: Results of Gaussian noise classified by neural networks. Neural networks classify the Gaussian noise to be either bird or cat. An element e_{ij} is the probability that the testing model i classifies the noise to class j .

Targeted Attack

The effect of generation in adversarial perturbations gets more pronounced in targeted attack mode for MNIST dataset. The experimental setup for targeted attack is the same as that of untargeted attack in MNIST, except κ , a parameter to tune the confidence of the source model towards the target class, is set to 20 in CW attack for better visualizing the results.

Figure 4 displays adversarial examples for both targeted BIM and CW attack algorithms. Figure 4(a) is the input images of 10 digits and the rest panels are adversarial examples with either SM or MM+G, where the maximum value of the adversarial perturbations is scaled to 1. The targets for digits (0,1,2,3,4,5,6,7,8,9) are chosen to be (6,7,4,5,9,3,8,9,0,4), respectively, so that, by modifying a portion of the input image, we can successfully transfer the input digit to the target digit.

In Figure 4 we see that adversarial perturbations eliminate existent (masking) and produce new (generation) recognizable characteristics with respect to input images, changing the class of an input image to the targeted class. Under SM, some of the adversarial examples can already be classified as the targeted classes, such as digits 0, 3, and 4 can be recognized as 6, 5, and 9, respectively, as shown in Figure 4(b) and (d). Under MM+G, more adversarial perturbations are

visually recognizable as targeted classes for both BIM and CW attack algorithms as shown in Figure 4(c) and (e), respectively. The produced characteristics, i.e., the effect of generation, supports our postulate that adversarial perturbations indeed contain human-recognizable information.

We further investigate whether, under the extreme situation where the input image is Gaussian noise, the property of generation still renders human-recognizable digits by employing targeted attack algorithms. Under SM, we have seen that the perturbations contain background noise and incomplete characteristics which makes the produced digits difficult to recognize. We have sent either a single or 100 different Gaussian noise(s) to 100 source models and averaged the resultant perturbations. This procedure minimizes noise and creates the full characteristics, leading to the emergence of recognizable digits. Visually examining Figure 5 reinforces our postulate that the perturbations indeed contain human-recognizable information.



Figure 4: Targeted attack illustrated by MNIST dataset. (a) Input images. (b) and (d) [(c) and (e)]: Adversarial perturbations under SM [MM+G] from BIM and CW attacks, respectively. Targets for digits (0,1,2,3,4,5,6,7,8,9) are (6,7,4,5,9,3,8,9,0,4), respectively. Under MM+G, many of the adversarial perturbations can easily be recognized as targeted classes for both attack algorithms.

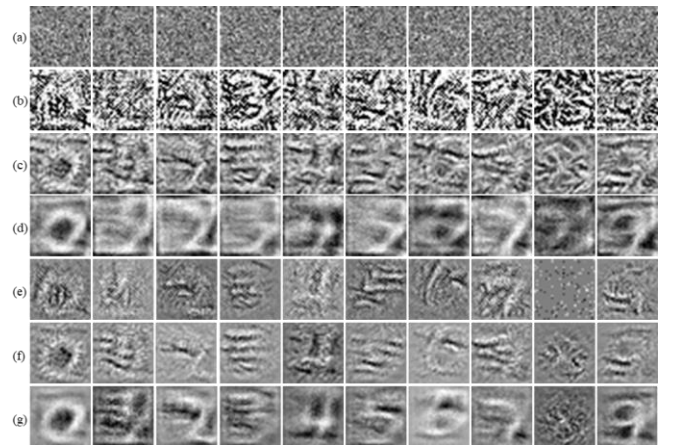


Figure 5: Adversarial perturbations produced by targeted attack algorithms with inputs as Gaussian noise. (a) Inputs of Gaussian noise. (b) Adversarial perturbations produced by targeted attack algorithms. The perturbations are visually recognizable as digits.

Gaussian noise. (b), (c), and (d) [(e), (f), and (g)]: Perturbations from BIM [CW] attack for 1 source model, 100 source models with identical input noise, and 100 source models with 100 different input noises, respectively. Recognizable digits emerge in the perturbations obtained from 100 source models.

Discussion

We have demonstrated that adversarial perturbations contain human-recognizable characteristics and these characteristics are responsible for fooling neural networks. Based on this postulate, important features regarding adversarial perturbations can be explained in a straightforward way.

(1) Network’s vulnerability against adversarial perturbations: For neural networks to correctly classify an input image, they put large gradient values on the recognizable characteristics when calculating the score of a labelled class. As mentioned before, a slight change of the pixel value can greatly influence neural networks’ prediction. This is consistent with our findings that vulnerability stems from small changes of recognizable characteristics in input images.

We have also found that the discrepancies of recognizable characteristics exist between adversarial perturbations and input images. The recognizable characteristics considered to be important by a neural network may not line up fully with those in the input image, instead they can have better alignment with adversarial perturbations since perturbations are produced directly from the neural network. Consequently, the discrepancies allow perturbations to play a larger role in the neural network’s classification process, a plausible explanation that neural network is vulnerable to adversarial perturbations.

(2) Transferability: The neural network must utilize some recognizable characteristics of an input image to identify this image correctly, for example, the face of a dog, the shapes of a car and a bird, as illustrated in Figure 1. Hence, for the purpose of classification, a good portion of the image’s recognizable characteristics likely overlap for different neural networks. If the overlapped characteristics are modified by the incorporation of adversarial perturbations, unrelated neural networks would still result in erroneous classifications.

(3) Adversarial training improving network’s interpretability: As long as the gradient of each class score remains roughly the same when adding perturbations to an input image (Goodfellow, Shlens, and Szegedy 2015), adversarial training in effect minimizes L_2 norm of the gradient for each class score (Simon-Gabriel et al. 2019). Since noise is included in the gradient, upon the minimization of L_2 norm, noise will be reduced. Minimizing L_2 norm can also help with recreating recognizable characteristics. We give an example to demonstrate this concept. Suppose two pixels are

equally important in a classification task, the inner product of the two pixels and corresponding gradients remains the same as long as the sum of the two gradients is fixed. However, L_2 norm reaches a minimum if the weights distribute equally on the two pixels. So neural networks will tend to distribute the values of the gradient equally. As a result, missing or less emphasized portions in the earlier gradient can now be reconstructed and this leads to a more complete information in the gradient. Thus, adversarial training is able to de-noise and recreate information in the gradient, similar to what we have shown earlier with MM+G, resulting in more recognizable perturbations.

(4) Non-trivial accuracy for classifiers trained by a perturbed dataset: Classifiers trained by a perturbed dataset and relabeled as the target class have demonstrated to achieve a non-trivial accuracy on a clean testing set. Our postulate explains this feature: Since adversarial perturbations contain human-recognizable characteristics, neural networks trained with a perturbed dataset retain the knowledge of those recognizable characteristics and therefore are able to attain non-trivial classification accuracy in clean data.

Conclusion

Adversarial perturbations have been shown to have a divergence between human perception and neural network’s judgement. Our work show that adversarial perturbations do contain human-recognizable information which is responsible for neural network’s misclassification.

The proposed algorithm, MM+G, allows us to observe the recognizable information hidden in the adversarial perturbations. Two properties are identified in adversarial perturbations: masking and generation. In addition, several interesting findings are presented in this work: the discrepancies between perturbations and input images, the aligning of perturbations from different attack algorithms, and the observation of missing cat which leads to the designation of complimentary class. The application of MM+G allows us to further investigate the working principles of neural networks and provides insights into devising defensive techniques against adversarial examples.

References

- Akhtar, N.; Mian, A.; Kardan, N.; and Shah, M. 2021. Advances in adversarial attacks and defenses in computer vision: A survey. *IEEE Access* **9**, 155161-155196.
- Carlini, N. and Wagner, D. 2017. Towards evaluating the robustness of neural networks. In *Symposium on Security and Privacy* 39–57.
- Eykholt, K. et al. 2018. Robust physical-world attacks on deep learning visual classification. In *Proc. International Conference on Computer Vision and Pattern Recognition* 1625-1634.
- Goodfellow, I.; Shlens, J.; and Szegedy, C. 2015. Explaining and harnessing adversarial examples. In *Proc. International Conference on Learning Representations*.
- Hinton, G. et al. 2012. Deep neural networks for acoustic modeling in speech recognition. *IEEE Signal Processing Magazine* **29**, 82–97.
- Ilyas, A. et al. 2019. Adversarial examples are not bugs, they are features. In *Proc. Advances in Neural Information Processing Systems* 32.
- Krizhevsky, A., and Hinton, G. 2009. Learning multiple layers of features from tiny images (Technical report). University of Toronto.
- Krizhevsky, A.; Sutskever, I.; and Hinton, G. 2012. ImageNet classification with deep convolutional neural networks. In *Proc. Advances in Neural Information Processing Systems* 25.
- Kurakin, A.; Goodfellow, I.; and Bengio, S. 2017. Adversarial examples in the physical world. In *International Conference on Learning Representations Workshop*.
- LeCun, Y., and Cortes, C. 2010. MNIST handwritten digit database. <http://yann.lecun.com/exdb/mnist>.
- LeCun, Y.; Bengio, Y.; and Hinton, G. 2015. Deep learning. *Nature* **521**, 436–444.
- Madry, A.; Makelov, A.; Schmidt, L.; Tsipras, D.; and Vladu, A. 2018. Towards deep learning models resistant to adversarial attacks. In *Proc. International Conference on Learning Representations*.
- Moosavi-Dezfooli, S.; Fawzi, A.; and Frossard, P. 2016. Deepfool: A simple and accurate method to fool deep neural networks. In *Proc. International Conference on Computer Vision and Pattern Recognition* 2574–2582.
- Moosavi-Dezfooli, S.; Fawzi, A.; Fawzi, O.; and Frossard, P. 2017. Universal adversarial perturbations. In *Proc. International Conference on Computer Vision and Pattern Recognition* 1765–1773.
- Papernot, N. et al. 2016. The limitations of deep learning in adversarial settings. In *European Symposium on Security and Privacy* 372–387.
- Papernot, N.; McDaniel, P.; and Goodfellow, I. 2016. Transferability in machine learning: From phenomena to black-box attacks using adversarial samples. *arXiv preprint arXiv:1605.07277*.
- Ross, A., and Doshi-Velez, F. 2018. Improving the adversarial robustness and interpretability of deep neural networks by regularizing their input gradients. In *Proc. Association for the Advancement of Artificial Intelligence* 32.
- Rumelhart, D.; Hinton, G.; and Williams, R. 1986. Learning representations by back-propagating errors. *Nature* **323**, 533-536.
- Samangouei, P.; Kabkab, M.; and Chellappa, R. 2018. Defensegan: Protecting classifiers against adversarial attacks using generative models. In *Proc. International Conference on Learning Representations*.
- Santurkar, S. et al. 2019. Image synthesis with a single (robust) classifier. In *Proc. Advances in Neural Information Processing Systems* 32.
- Schmidt, L.; Santurkar, S.; Tsipras, D.; Talwar, K.; and Madry, A. 2018. Adversarially robust generalization requires more data. In *Proc. Advances in Neural Information Processing Systems* 31.
- Shafahi, A.; Huang, W.; Studer, C.; Feizi, S.; and Goldstein, T. 2019. Are adversarial examples inevitable? In *Proc. International Conference on Learning Representations*.
- Simonyan, K.; Vedaldi, A.; and Zisserman, A. 2014. Deep inside convolutional networks: Visualising image classification models and saliency maps. In *International Conference on Learning Representations Workshop*.
- Simon-Gabriel, C.; Ollivier, Y.; Bottou, L.; Schölkopf, B.; and Lopez-Paz, D. 2019. First-order adversarial vulnerability of neural networks and input dimension. In *Proc. International Conference on Machine Learning* 5809-5817.
- Smilkov, D.; Thorat, N.; Kim, B.; Viégas, F.; and Wattenberg, M. 2017. Smoothgrad: Removing noise by adding noise. In *Workshop on Visualization for Deep Learning*.
- Song, Y.; Kim, T.; Nowozin, S.; Ermon, S.; and Kushman, N. 2018. Pixeldefend: Leveraging generative models to understand and defend against adversarial examples. In *Proc. International Conference on Learning Representations*.
- Su, J.; Vargas, D.; and Sakurai, K. 2019. One pixel attack for fooling deep neural networks. *IEEE Transactions on Evolutionary Computation* **23**, 828–841.
- Szegedy, C. et al. 2014. Intriguing properties of neural networks. In *Proc. International Conference on Learning Representations*.
- Tanay, T., and Griffin, L. 2016. A boundary tilting perspective on the phenomenon of adversarial examples. *arXiv preprint arXiv:1608.07690*.
- Tramèr, F.; Papernot, N.; Goodfellow, I.; Boneh, D.; and McDaniel, P. 2017. The space of transferable adversarial examples. *arXiv preprint arXiv:1704.03453*.
- Tsipras, D.; Santurkar, S.; Engstrom, L.; Turner, A.; and Madry, A. 2019. Robustness may be at odds with accuracy. In *Proc. International Conference on Learning Representations*.

Supplementary Material

Detailed Experimental Setup

Framework

We have conducted the experiments on both MNIST and CIFAR10 datasets. Two datasets have different experimental setups. The code implementation relies heavily on PyTorch (Paszke et al. 2019) and the attack algorithms are based on torchattacks (Kim 2020).

Model Architecture

MNIST: All models (101 models) used for source and testing models are self-trained models with the same VGG-like architecture (Simonyan and Zisserman 2014) but different random seeds. Initialization weight distribution follows PyTorch default settings.

CIFAR10: All models used for CIFAR10 are downloaded from PyTorchCV (Oleg Sémary) (70 models total). Under MM+G, models in source models are completely different from those in the testing models. Under SM, the source model ResNet (He et al. 2016) is the same model as that in the testing model. The model architecture is listed in Table S1.

Dataset		MNIST	CIFAR10
Category	Source models / MM+G	VGG-like models \times 100	66 models in PyTorchCV
	Source model / SM	VGG-like model	ResNet-56
	Testing models	VGG-like model	DenseNet-BC-40_k24, DIA-ResNet-164, PyramidNet-110_a48, ResNet-56
Attack parameters	BIM	iterations=50, $\epsilon=0.2$, $\alpha=0.008$	iterations=50, $\epsilon=0.03$, $\alpha=0.0012$
	CW	$C=0$, $\kappa=0$, steps=1000, $\eta=0.01$	$C=0$, $\kappa=0$, steps=1000, $\eta=0.01$
	DeepFool	overshoot=0.02, steps=50	overshoot=0.02, steps=50
Gaussian noise	Number of copies (n)	20	BIM, CW: 100, DeepFool: 20
	Standard deviation (σ)	0.2	BIM, CW: 0.05, DeepFool: 0.1

Table S1: Information for experimental settings.

Selected Data

We have selected the first 10 images from each class for all 10 classes in the testing sets of CIFAR10 and MNIST to give a total of 200 selected images, and obtained respective adversarial perturbations under SM and MM+G.

Modification on Attack Algorithms

Adding noise to input images will alter neural network’s class score. This may affect crafted adversarial perturbations as well as the order of the classes, which would lead to the misclassification of the input image. In some algorithms,

misclassification of the input image will make the algorithms fail to initiate and the class with the second highest score would be designated as the target class, which may have been rearranged due to the presence of noise. As a result, noise would lead to a different target class for these algorithms. To mitigate this noise effect, modification needs be applied to attack algorithms.

The modification we have employed is to calibrate the class score to the score in the absence of noise. Mathematically, this means

$$M'(x + N(0, \sigma^2) + V(x)) = M(x + N(0, \sigma^2) + V(x)) + \text{calibrator}, \\ \text{calibrator} = M(x) - M(x + N(0, \sigma^2)).$$

where $M(x)$ and $M'(x)$ are the original and the calibrated class score for a given image x , respectively; $N(0, \sigma^2)$ is Gaussian noise with mean 0 and variance σ^2 , and $V(x)$ is the adversarial perturbations calculated from the input image x .

Attack Parameters

The information of three attack algorithms is listed in Table S1. The attack parameters for CW and DeepFool attack on MNIST and CIFAR10 are identical. For BIM attack, ϵ is set at 0.2 for MNIST and 0.03 for CIFAR10.

Gaussian Noise

The information of incorporating Gaussian noise with input images under MM+G is listed in Table S1. We have incorporated different Gaussian noises to individual input images to increase the number of perturbations. For Gaussian noise employed in MNIST dataset, the standard deviation is 0.2 and the number of copies is 20. For BIM and CW attacks in CIFAR10 the standard deviation is 0.05 and the number of copies is 100. Since DeepFool attack requires more time to produce perturbations, we set the number of copies to 20 and empirically found that increasing the standard deviation of Gaussian noise to 0.1 makes the adversarial perturbations more visible for DeepFool attack in CIFAR10.

Effect of Clipping

A standard procedure of processing adversarial examples is to clip the pixel values to the range between 0 and 1. This procedure is not followed for adversarial perturbations V_i in Eqn. (1) because clipping will affect the perceptibility of perturbations.

Processing Adversarial Perturbations

We have evaluated the attack strength of adversarial perturbations by multiplying a quantity ϵ with their signs. However, this might lead to noisy adversarial perturbations. To reinforce that the recognizable characteristics in adversarial

perturbations under MM+G are the key conspirator for fooling neural networks, we modify the way of processing adversarial perturbations by retaining only human-recognizable information and eliminating the noise. This is summarized below:

$$V' = \begin{cases} \varepsilon \cdot \text{sign}(V) & \text{if } |V| > 0.8 \times \text{avg}(|V|). \\ 0 & \text{otherwise.} \end{cases}$$

Here V and V' are the original and processed adversarial perturbations, respectively. $\varepsilon = 0.03$ for CIFAR10. The average accuracy for testing models drops from 94% for input images to 20% for CW attack in CIFAR10 dataset under this method. The effect of noise can be further investigated by setting noise, i.e., $V' = 0$, to be either $+\varepsilon$ or $-\varepsilon$ with equal probability. This leads to a slight drop of average accuracy to 16%, indicating that recognizable information, not noise, is critical for fooling neural networks. The results are illustrated in Figure S1.

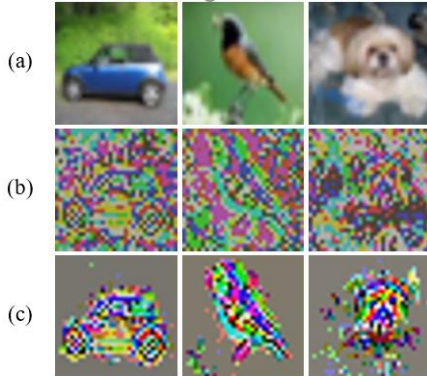


Figure S1: Processing adversarial perturbations. (a) Input images. (b) Perturbations under MM+G are processed by multiplying a quantity ε with their signs. (c) The method of processing adversarial perturbations is identical to that of (b) except that perturbation values smaller than the averaged absolute value are set to 0. Adversarial perturbations after eliminating noise still demonstrate the ability of attack, indicating the key conspirator for fooling neural networks is human-recognizable information.

Visualizing Adversarial Examples

Adversarial examples, processed by Eqn. (2), are shown in Figure S2. Figure S2(a) shows input images and (b), (c), and (d) are adversarial examples derived from different attack algorithms. Though the differences between input images and adversarial examples are not significant enough to influence human’s judgement on classifying individual images, the perturbations are sufficient to fool testing models.

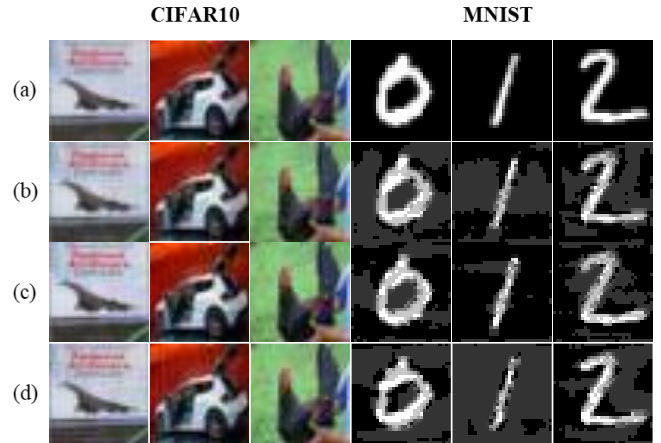


Figure S2: Incorporation of adversarial perturbations with input images from CIFAR10 and MNIST datasets. (a) Input images. (b), (c), and (d): Adversarial examples from BIM, CW and DeepFool attacks, respectively.

Producing Perturbations from Noise

In Figure 5 of main text where inputs are Gaussian noise, we have observed human-recognizable digits emerge in adversarial perturbations. Intriguingly, digits obtained by averaging 100 adversarial perturbations produced from a single Gaussian noise have sharp edges and large background streaks/wringers compared to those obtained from 100 Gaussian noises. A digit with a sharp edge implies that perturbations produced from the same Gaussian noise by 100 models are similar to each other. The appearance of large background streaks/wringers again illustrates this effect of similarity. If models’ weights are uncorrelated, the degrees of similarity of the perturbations for 1 and 100 input Gaussian noise(s) should be the same since noise does not contain any information. With the streaks/wringers showing up, it implies that source models starting from different initialization weights ultimately lead to similar weights.

Further Investigation on MM+G

Under MM+G, we have performed the double summations to obtain adversarial perturbations. Here we demonstrate the usefulness of doing a single summation, namely, to obtain the perturbations through the single-model setting with Gaussian noise (SM+G), averaging 1 to n in Eqn. (1). For brevity, we only show the results from BIM attack in the following discussion. In Figure S3 we see that human-recognizable characteristics produced under SM+G emerge in the perturbations. Compared with perturbations from MM+G, shown in Figure S3, recognizable characteristics in perturbations from SM+G is less complete. SM+G reduces the effect of noise but cannot recreate the complete characteristics, hence the attack transferability is not strong. Since

SM+G allows us to observe human-recognizable perturbations produced by a single neural network and these perturbations plays a dominant role in the classification of the neural network, it can be a new tool for understanding the working principles of the neural network.

We further demonstrate the usefulness of another summation in Eqn. (1), namely, to obtain the perturbations through multiple models, i.e., averaging 1 to m , without adding Gaussian noise (MM). Figure S4(b) and (d) shows the perturbations from MM. Perturbations from MNIST dataset, Figure S4(b), contain human-recognizable digits and those of CIFAR10, Figure S4(d), contain visible but coarse con-

tours of the input images. They show that, without noise, recognizable perturbations are still attainable.

We have also studied the influences of the number of copies, n , and the standard deviation, σ , on adversarial perturbations by employing SM+G. In Figure S5 we see that, with the increase of n , the noise in perturbations becomes smaller and the contours emerge gradually. The gradual emergence of the contours again confirms our postulate that the recognizable characteristics exist in adversarial perturbations. A large standard deviation will make the shape of recognizable characteristics in adversarial perturbations less clear and grid-like patterns emerge, as shown in Figure S6.

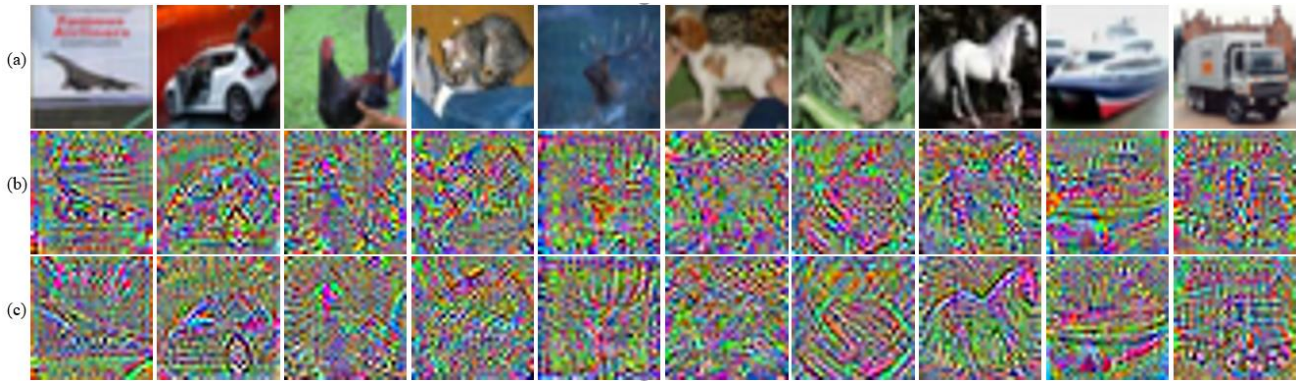


Figure S3: Perceptibility of adversarial perturbations under SM+G. (a) Input images. (b) Perturbations under SM+G with $n = 1000$, $\sigma = 0.05$. (c) Perturbations under MM+G with $n = 20$, $\sigma = 0.05$. Averaging sufficient number of copies allows us to visualize adversarial perturbations even for a single source model, as shown in (b). Compared with perturbations under MM+G, the shape of the recognizable characteristics is less complete under SM+G.



Figure S4: Adversarial perturbations from MM. (a) and (c): Input images from MNIST and CIFAR10 datasets, respectively. (b) and (d): Adversarial perturbations under MM. Clear digits can be seen in the adversarial perturbations for images from MNIST. Coarse but visible contours can be observed in perturbations for CIFAR10 images.

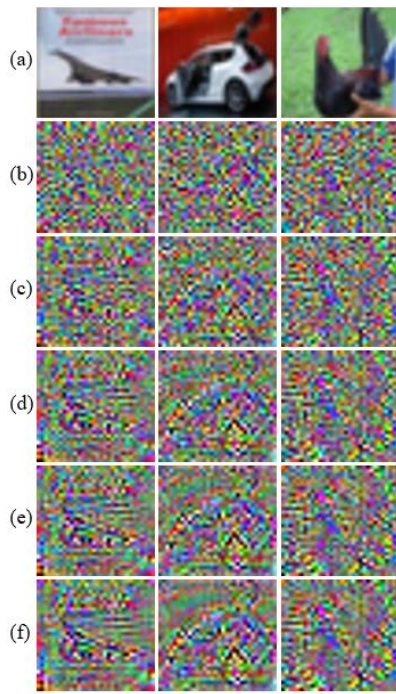


Figure S5: Perceptibility vs. number of perturbations under SM+G. (a) Input images. (b)-(f): Perturbations under SM+G with $n = 5, 20, 50, 100$ and 1000 , respectively. With the increase of the number of copies, the noise becomes smaller and the contours get clearer progressively.

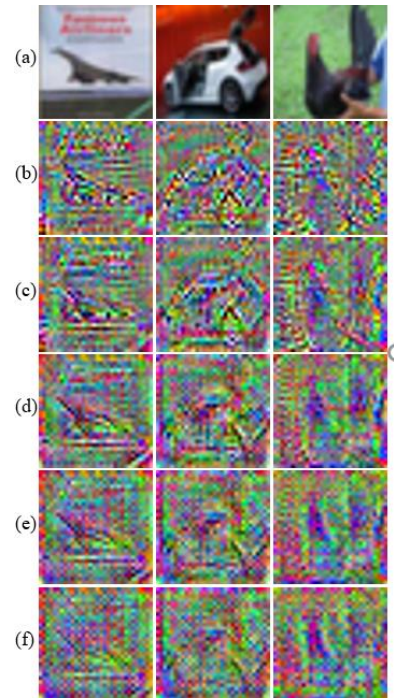


Figure S6: Adversarial perturbations vs. standard deviation under SM+G. (a) Input images. (b)-(f): Perturbations under SM+G with $\sigma = 0.05, 0.1, 0.2, 0.3$ and 0.4 , respectively. A large standard deviation makes the shape of recognizable characteristics in adversarial perturbations less clear and produces grid-like patterns. Number of copies $n = 1000$.

References

He, K.; Zhang, X.; Ren, S.; and Sun, J. 2016. Deep residual learning for image recognition. In *Proc. Computer Vision and Pattern Recognition* 770-778.

Kim, H. 2020. Torchattacks: A PyTorch repository for adversarial attacks. *arXiv preprint arXiv:2010.01950*.

Oleg Sémary. Computer vision models on PyTorch. <https://github.com/osmr/imgclsmob>

Paszke, A. et al. 2019. PyTorch: An imperative style, high-performance deep learning library. In *Proc. Advances in Neural Information Processing Systems* 32.

Simonyan, K. and Zisserman, A. 2014. Very deep convolutional networks for large-scale image recognition. *arXiv preprint arXiv:1409.1556*.